Analytical investigation of revival phenomena in the finite square-well potential

David L. Aronstein* and C. R. Stroud, Jr.

The Institute of Optics, University of Rochester, Rochester, New York 14627

(Received 17 December 1999; revised manuscript received 6 March 2000; published 6 July 2000)

We present an analytical investigation of revival phenomena in the finite square-well potential. The classical motion, revival, and super-revival time scales are derived exactly for wave packets excited in the finite well. These time scales exhibit a richer dependence on wave-packet energy and on potential-well depth than has been found in other quantum systems: They explain, for example, the difficulties in exciting wave packets with strong classical features at the bottom of a finite well, or with clearly resolved super-revivals in a shallow well. In the proper regions of validity, the time scales predict the instances of wave-packet reformation extremely accurately. Revivals at the bottom of the well are explored as a ''universal'' limit of the general theory, which offers the clearest connection with the series of fractional and full revivals seen in the dynamics of the infinite square-well potential.

PACS number(s): 03.65.Ge, 42.50.Md, 73.20.Dx, 02.30.Mv

I. INTRODUCTION

Quantum wave packets can be excited with strong classical properties, which move as localized entities along the trajectories predicted by classical mechanics [1]. In time, such wave packets spread out and decay, losing their signatures of classical motion. Later in the dynamics, however, there are a series of *fractional* and *full* revivals, windows of time in which the wave-packet shape and classical motion resurface [2]. The revival windows in turn decay away, but at even longer times the classical behavior reappears in a series of *super*-revivals [3]. The primary purpose of this paper is to present an analytical investigation of such classical motion and revival phenomena in the quantum evolution of a particle confined in the finite square-well potential.

In the theory of revival phenomena, the discrete energy spectrum E_n of a quantum system (here assumed to depend on a single quantum number n [4]) is studied in the immediate vicinity of a wave packet's mean quantum number $\bar{n}$. The time scales T_1, T_2, and T_3, appearing in the Taylor-series expansion of the energies when written in the form

$$E_n = E_{\bar{n}} + 2\pi\hbar \left[\frac{(n-\bar{n})}{T_1} + s_2 \frac{(n-\bar{n})^2}{T_2} + s_3 \frac{(n-\bar{n})^3}{T_3} + \cdots \right] \tag{1}$$

characterize the wave packet's classical motion, revivals, and super-revivals, respectively [5]. (The signs $s_j = \pm 1$ are adjusted to insure that times T_j are positive, with $s_1 = +1$ in general.) These times are related to derivatives of the energy spectrum evaluated at $n = \bar{n}$, so wave packets of different energies usually have different revival times.

The energy levels of the *infinite* square-well potential [6] vary quadratically with quantum number, $E_n = E_1 n^2$. This has the polynomial form sought by Eq. (1), whether it is written as

$$E_n = 2\pi\hbar \left[\frac{n^2}{\tau_2} \right] \tag{2}$$

or as

$$E_n = E_{\bar{n}} + 2\pi\hbar \left[\frac{(n-\bar{n})}{T_1} + \frac{(n-\bar{n})^2}{T_2} \right]. \tag{3}$$

These equations serve as the foundation for two alternate, but fully compatible, descriptions of revival phenomena in the infinite well. The direct polynomial description of Eq. (2) predicts exactly periodic dynamics with period $\tau_2 = 2\pi\hbar/E_1$. The Taylor series regrouping of Eq. (3) describes a classical motion period $T_1 = 2\pi\hbar/(2\bar{n}E_1)$ and a revival time $T_2 = \tau_2 = 2\pi\hbar/E_1$. At time T_2 there has been one revival period and $T_2/T_1 = 2\bar{n}$ periods of classical motion; thus (for integer $\bar{n}$) these time scales are synchronized and again there is periodic dynamics.

We emphasized Eq. (2) and the ''universal'' time scale τ_2 in an analysis of the infinite square well [7]. Time τ_2 is universal in that it does not depend on the mean quantum number $\bar{n}$, so wave packets of all energies revive at the same time. By focusing on this description instead of that of Eq. (3), we avoided analyzing the classical motion (T_1) dynamics of low-energy or poorly localized wave packets that show no obvious connection with classical mechanics.

Recently, Venugopalan and Agarwal [8] investigated wave packets excited in the *finite* square well, and showed that the periodicity of the dynamics and the exactness of the revivals are broken by the finite potential depth. They demonstrated that such wave packets exhibit super-revival phenomena, absent in the infinite well. The authors compared numerical calculations of the finite square-well dynamics (studied as functions of the initial wave packet and of the potential-well depth) with the dynamics of the anharmonic oscillator (for which the energy spectrum is known in closed form). However, their work lacked a direct analytic description of the finite square-well revival phenomena.

In this paper, we derive the finite square-well revival times exactly, despite the transcendental nature of the quan-

---

*Electronic address: daron@optics.rochester.edu

tization equation describing the bound energy levels. We show that the two alternate views of the infinite square-well dynamics separate into distinct models for wave packets in the finite well: ''Mean-quantum-number'' revivals, which follow the regime outlined in Eqs. (1) and (3), describe revival phenomena throughout the well, failing only for wave packets excited too close to the continuum at the top of the well. ''Universal'' revivals, which generalize the approach of Eq. (2), are a limiting case that pertain to wave packets excited at the bottom of the well, offering the clearest connection with the dynamics seen in the infinite square well.

II. FINITE SQUARE-WELL SYSTEM

We consider wave packets excited in the finite square well, so it is useful to review the notation and standard results for this system. The one-dimensional finite square-well potential in quantum mechanics confines a nonrelativistic particle of mass m to a box of length L and potential depth V_0 and is described by

$$V(x) = \begin{cases} 0, & |x| \leq L/2 \\ V_0, & |x| > L/2. \end{cases} \quad (4)$$

Popular quantum mechanics textbooks [9] give excellent elementary treatments of this problem. It proves useful to analyze the system in terms of two dimensionless quantities (using notation from Barker *et al.* [10]): the *scaled action* α depends on the particle energy E with

$$\alpha = \frac{\sqrt{2mE}}{\hbar} \frac{L}{2}, \quad (5)$$

and the *well-strength parameter* P depends on the potential depth V_0 with

$$P = \frac{\sqrt{2mV_0}}{\hbar} \frac{L}{2}. \quad (6)$$

The discrete bound-state energy eigenfunctions $\phi_n(x)$, found by solving the time-independent Schrödinger equation in each region of constant potential separately, are superpositions of left- and right-traveling waves inside the well and attenuating waves outside. The conditions for the quantization of the energy levels supported by the square well are found by examining the continuity of $\phi_n(x)$ and $\phi'_n(x)$ at the well boundaries ($x = \pm L/2$). Sprung, Wu, and Martorell [11] discovered a remarkably simple expression for this quantization condition: the bound energies are solutions of the equation

$$\alpha + \sin^{-1}\left(\frac{\alpha}{P}\right) = \frac{n\pi}{2}, \quad (7)$$

which relates the scaled action α to the quantum number n for a given well strength P. Choosing the branch $-\pi/2 \leq \sin^{-1}(\alpha/P) \leq \pi/2$ of the multivalued arcsine function, the ground state (the lowest positive solution α) corresponds to

the quantum number $n=1$. Note that the number of bound levels $n_{\max}$ supported by the well is

$$n_{\max} = \text{int}\left(\frac{P}{\pi/2}\right) + 1 \quad (8)$$

[with int(x) equal to the largest integer smaller than x]; thus the quantization equation (7) has a unique solution α for each quantum number $n \in \{1, 2, \cdots, n_{\max}(P)\}$.

We assume that the particle's wave function is a coherent superposition of bound energy levels centered around mean quantum number $\bar{n}$. The initial wave-packet state is written as $|\psi(t=0)\rangle$ and its projection onto the nth energy level as $c_n = \langle \phi_n | \psi(t=0) \rangle$. Thus the time evolution of the wave packet is

$$\psi(x,t) = \sum_{n=1}^{n_{\max}} \exp[-iE_n t/\hbar] c_n \phi_n(x). \quad (9)$$

A natural unit of energy in square-well problems is $\hbar^2/mL^2$, and the corresponding unit of time is $mL^2/\hbar$. These units are assumed and suppressed throughout this paper.

III. ''MEAN-QUANTUM-NUMBER'' REVIVALS

In this section, we compute the wave-packet expansion of the finite square-well energies in the form of Eq. (1). This provides expressions for the wave-packet time scales, which we explore in detail. With knowledge of these time scales, we connect the square-well wave-packet dynamics with the larger theory of revival phenomena, to make highly accurate predictions of the dynamics in this system.

A. Wave-packet expansion and time scales

A wave packet excited in the vicinity of mean quantum number $\bar{n}$ is associated with a mean scaled action $\alpha_{\bar{n}}$, via Eq. (7), and a mean energy $E_{\bar{n}}$, via Eq. (5). We examine the quantization equation (7) in this vicinity by expanding the arcsine function in a Taylor series around $\alpha = \alpha_{\bar{n}}$. We find that

$$\frac{(n-\bar{n})\pi}{2} = (\alpha - \alpha_{\bar{n}}) + \frac{1}{\left[1 - \left(\frac{\alpha_{\bar{n}}}{P}\right)^2\right]^{1/2}} \left(\frac{\alpha - \alpha_{\bar{n}}}{P}\right)$$

$$+ \frac{\frac{\alpha_{\bar{n}}}{P}}{2\left[1 - \left(\frac{\alpha_{\bar{n}}}{P}\right)^2\right]^{3/2}} \left(\frac{\alpha - \alpha_{\bar{n}}}{P}\right)^2$$

$$+ \frac{1 + 2\left(\frac{\alpha_{\bar{n}}}{P}\right)^2}{6\left[1 - \left(\frac{\alpha_{\bar{n}}}{P}\right)^2\right]^{5/2}} \left(\frac{\alpha - \alpha_{\bar{n}}}{P}\right)^3 + \cdots . \quad (10)$$

This equation relates the shifted quantum number $(n-\bar{n})$ to a power series in $(\alpha-\alpha_{\bar{n}})$. With an eye toward Eq. (1), we invert this equation to describe $(\alpha-\alpha_{\bar{n}})$ as a power series in $(n-\bar{n})$ using the power-series inversion theorem [12], and compute the energy spectrum near $E=E_{\bar{n}}$ using Eq. (5). We find that

$$E_n = E_{\bar{n}} + \frac{4\alpha_{\bar{n}}[P^2-\alpha_{\bar{n}}^2]^{1/2}}{1+[P^2-\alpha_{\bar{n}}^2]^{1/2}}\left[\frac{(n-\bar{n})\pi}{2}\right]$$

$$+2\frac{(P^2-2\alpha_{\bar{n}}^2)+[P^2-\alpha_{\bar{n}}^2]^{3/2}}{(1+[P^2-\alpha_{\bar{n}}^2]^{1/2})^3}\left[\frac{(n-\bar{n})\pi}{2}\right]^2$$

$$-\frac{8\alpha_{\bar{n}}}{3}\frac{(P^2-\frac{1}{4}\alpha_{\bar{n}}^2)+[P^2-\alpha_{\bar{n}}^2]^{1/2}}{(1+[P^2-\alpha_{\bar{n}}^2]^{1/2})^5}\left[\frac{(n-\bar{n})\pi}{2}\right]^3-\cdots.$$

$$(11)$$

Equation (11) has the same form as the standard wave-packet expansion, Eq. (1), so from it we extract the wave-packet times: The classical motion time scale is

$$T_1 = \frac{1+[P^2-\alpha_{\bar{n}}^2]^{1/2}}{\alpha_{\bar{n}}[P^2-\alpha_{\bar{n}}^2]^{1/2}}, \qquad (12)$$

the revival time scale is

$$T_2 = \frac{4}{\pi}\left|\frac{(1+[P^2-\alpha_{\bar{n}}^2]^{1/2})^3}{(P^2-2\alpha_{\bar{n}}^2)+[P^2-\alpha_{\bar{n}}^2]^{3/2}}\right| \qquad (13)$$

(with $s_2=\pm1$, discussed later), and the super-revival time scale is

$$T_3 = \frac{6}{\pi^2}\frac{(1+[P^2-\alpha_{\bar{n}}^2]^{1/2})^5}{(\alpha_{\bar{n}}P^2-\frac{1}{4}\alpha_{\bar{n}}^3)+\alpha_{\bar{n}}[P^2-\alpha_{\bar{n}}^2]^{1/2}} \qquad (14)$$

(with $s_3=-1$). Higher-order time scales (T_4, etc.) are readily computed by continuing the expansion (10) and retaining additional terms in the inverted series for $\alpha_{\bar{n}}$ and $E_{\bar{n}}$.

Equations (12)–(14) are *exact*. To elaborate, note that the exact expression for the classical motion time scale (for example), found by comparing Eq. (1) with the standard form for a Taylor expansion, is

$$\frac{1}{T_1} = \frac{1}{2\pi\hbar}\frac{dE}{dn}\bigg|_{n=\bar{n}}. \qquad (15)$$

Thus T_1 can be found using the relationships between the energy E and the scaled action α in Eq. (5), and between α and the quantum number n in Eq. (7). We find this procedure to be cumbersome, especially when generalized to find T_2 and higher-order time scales. The method presented above, using the power-series inversion theorem, offers a clear path through such calculations without introducing any approximations.
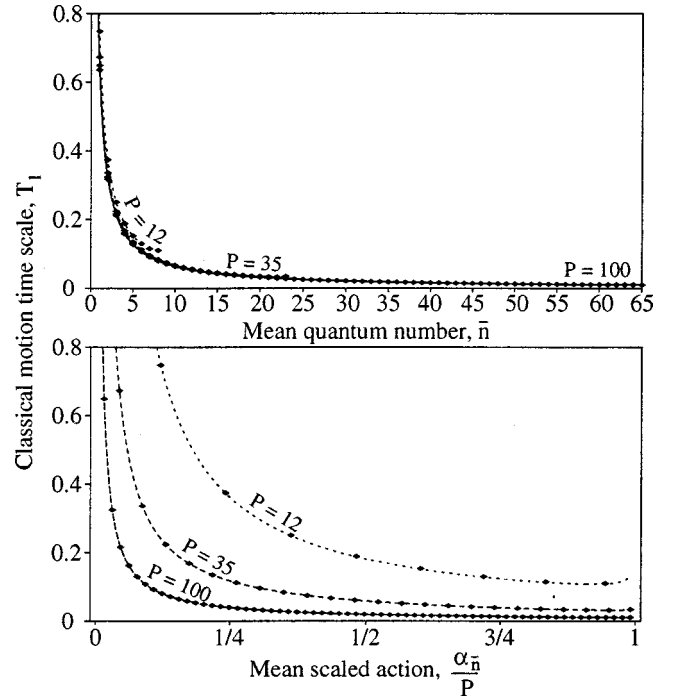

FIG. 1. Time scale T_1: the classical motion time scale as a function of mean quantum number $\bar{n}$ and as a function of mean scaled action $\alpha_{\bar{n}}/P$ for well-strength parameters $P=12$, 35, and 100.

The key point is that the wave-packet time scales are analytic functions of the scaled action $\alpha_{\bar{n}}$, but not of the quantum number $\bar{n}$. For a given wave packet, the connection between $\alpha_{\bar{n}}$ and $\bar{n}$ is established by solving the transcendental equation (7) numerically, then the time scales (12)–(14) are found with this numerical value of $\alpha_{\bar{n}}$.

B. Exploration of time scales

Plots of the wave-packet time scales are shown in Figs. 1–3 for well strengths of $P=12$, 35, and 100. We show each time scale in two complementary ways: as a function of mean quantum number $\bar{n}$ (to study the dependence on the well depth for a given energy level) and as a function of mean scaled action $\alpha_{\bar{n}}/P$ (to study the time scales at the *bottom, middle,* and *top* of wells of different depths). There are only n_{max} discrete energy levels for a given well-strength parameter, but the wave packet's mean quantum number or scaled action need not be restricted to this finite spectrum. For this reason, each plot shows the time scales as continuous quantities (of $\bar{n}$ or $\alpha_{\bar{n}}/P$) with small dots placed at the stationary solutions. Note that plots with respect to quantum number have a domain of $1\leq n\leq n_{max}$, so different well strengths have different domains, whereas plots with respect to scaled action are defined on the domain $0\leq\alpha_{\bar{n}}/P\leq1$ for all values of well strength.

The classical motion time scale T_1 (Fig. 1) falls off rapidly with increasing quantum number or scaled action. To connect this with intuition from classical mechanics, note that a classical particle with energy $E_{\bar{n}}$ travels at speed
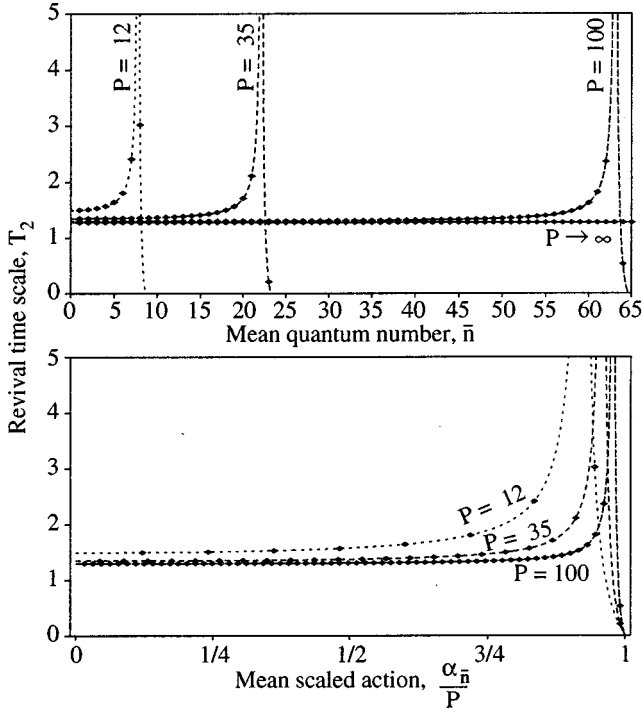
FIG. 2. Time scale T_2: the revival time scale as a function of mean quantum number $\bar{n}$ and as a function of mean scaled action $\alpha_{\bar{n}}^-/P$ for well-strength parameters $P = 12$, 35, and 100.

FIG. 3. Time scale T_3: the super-revival time scale as a function of mean quantum number $\bar{n}$ and as a function of mean scaled action $\alpha_{\bar{n}}^-/P$ for well-strength parameters $P = 12$, 35, and 100.

$v = \sqrt{2E_n^-/m}$ and completes one roundtrip inside the well in time

$$T_{\text{rt}} = \frac{2L}{v} = \frac{1}{\alpha_{\bar{n}}^-}. \tag{16}$$

Times T_1 and T_{rt} are nearly equal (with $T_{\text{rt}} < T_1$) and are reconciled by describing the classical motion in a larger well of length $L + \delta L$, with

$$\delta L = \frac{L}{[P^2 - \alpha_n^{-2}]^{1/2}}. \tag{17}$$

This length correction δL depends on both well strength and wave-packet energy and serves as the "penetration depth" (or "tunneling depth") beyond the square-well boundaries. Equation (17) generalizes the $\alpha_n^- = 0$ limit of δL due to Barker *et al.* [10], found by examining the energy levels at the well bottom.

The revival time scale T_2 (Fig. 2) is equal to $(4/\pi)(P+1)^2/P^2$ at the well bottom and does not vary significantly throughout most of the well. This weak dependence on quantum number is the key to the universal revival limit analyzed in Sec. IV. Near the top of the well, however, T_2 diverges, and at the very top it falls to zero. The quantity inside the absolute value in Eq. (13) switches sign at this divergence, with $s_2 = +1$ below and $s_2 = -1$ above it.

There is the intriguing possibility of *revival suppression* for wave packets excited with $T_2 \rightarrow \infty$. Such wave packets evolve from their classical motion directly to super-revival
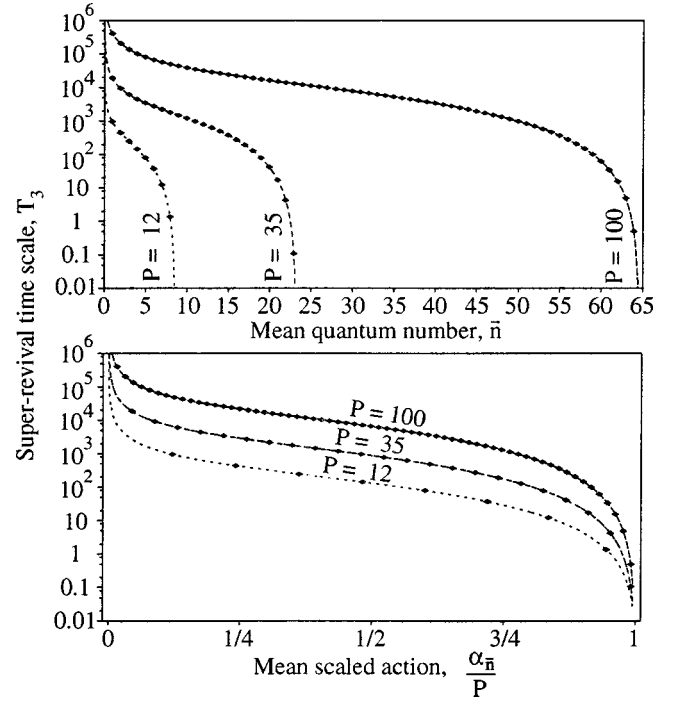
dynamics, and this behavior has not been predicted in any other quantum system. Unfortunately, for modest values of the well-strength parameter (e.g., the values considered in Fig. 2), the revival time divergence occurs between levels $n_{\max} - 1$ and $n_{\max}$, too close to the continuum limit to be pertinent for wave-packet states. For extremely deep wells ($P \gg 1000$), the divergence in T_2 does occur below level $n_{\max} - 1$; wave-packet states excited in this vicinity are possible in principle, but it seems implausible to excite such a state in a physical system in practice. For the rest of this paper we limit our attention to wave packets excited below the T_2 divergence.

The super-revival time scale T_3 (Fig. 3) varies monotonically from $T_3 \rightarrow \infty$ at the well bottom to $T_3 \rightarrow 0$ at the well top. The super-revival time depends strongly on well strength, unlike the classical motion and revival times; for example, at the well bottom it scales as $T_3 \propto (P+1)^5/P^2 \sim P^3$.

C. Semiclassical time-scale hierarchy

The wave-packet time scales of highly excited quantum systems usually satisfy a hierarchy [5]

$$T_1 \ll T_2/2! \ll T_3/3! \ll \cdots, \tag{18}$$

and, broadly speaking, a given wave packet has well-resolved classical motion, revivals, and super-revivals when these conditions are met. With Rydberg atomic-electron wave packets [13], for example, this is satisfied in the high-energy (semiclassical) limit and the inequalities become stronger with increasing $\bar{n}$. In the finite square-well system,
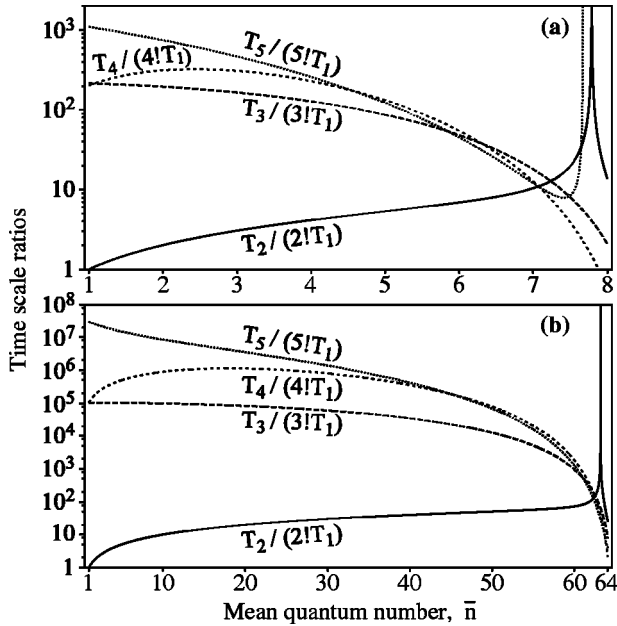
FIG. 4. Time-scale ratios: $T_j/(j!T_1)$ as a function of mean quantum number $\bar{n}$ for (a) $P=12$ and (b) $P=100$.

the presence of a maximum quantum number n_{max} (for fixed well strength P) has a dramatic impact on the regime in which the various inequalities in the time-scale hierarchy are satisfied. We study this in Fig. 4, showing the time-scale ratios $T_j/(j!T_1)$ as functions of the mean quantum number for $P=12$ and $P=100$.

At the top of the well (as $\bar{n} \to n_{max}$), the time-scale ratios drop precipitously and the hierarchy (18) is not satisfied. The usual formulation of revival theory does not apply to the dynamics of wave packets excited here, so we do not explore this regime further. We note, however, that a detailed study of the behavior at the well top is important for problems involving the scattering of continuum wave packets excited *above* the well [14].

The inequality $T_1 \ll T_2/2$ does not hold at the bottom of the well (with $T_2/T_1 \approx 2$ at $\bar{n}=1$ for all well strengths). Thus the classical motion and revival dynamics cannot be separated for wave packets at the well bottom; this is explored more carefully in Sec. IV B. For shallow wells [e.g., Fig. 4(a)] the inequality is not satisfied in any part of the well (except where T_2 diverges). For deeper wells [with $P \gtrsim 20$, e.g., Fig. 4(b)], the inequality becomes valid away from the bottom, and wave-packet states exhibiting classical motion can be excited for $\bar{n} \gtrsim 10$.

The inequality $T_2/2! \ll T_3/3!$ holds beautifully, even for shallow wells with only a few bound states. Wave-packet revivals are the most prominent and well-resolved feature in square-well dynamics, across the range of possible wave-packet shapes and energies.

The inequality $T_3/3! \ll T_4/4!$ is not met for shallow wells [e.g., Fig. 4(a)]. For deeper wells [with $P \gtrsim 60$, e.g., Fig. 4(b)], the inequality holds near the middle of the well and wave-packet super-revivals become observable. However, the inequality $T_4/4! \ll T_5/5!$ is never satisfied in this region
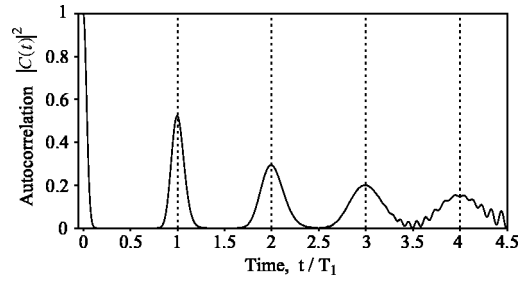

FIG. 5. Classical motion dynamics: autocorrelation function $|C(t)|^2$ of the Gaussian wave packet described in Sec. III D, during the first several periods of classical motion. The dashed vertical lines are drawn at multiples of T_1, the predicted classical period.

[with $T_5/(5T_4) \approx 95/14\pi \approx 2.16$ at $\alpha_{\bar{n}}^-/P = 1/2$ for all well strengths], and the cumulative effects of T_4 and T_5 interference lead to rather poor super-revivals for the well strengths considered. This is quite different than for Rydberg wave packets, in which the initial wave-packet shape is better replicated during the super-revivals than at the revivals.

There is no simple conclusion for how the full semiclassical hierarchy can best be fulfilled in the finite square well. On one hand, the time scales T_3, T_4, and T_5 are as far apart from each other as possible near the bottom of the well: In Fig. 4, we estimate that this occurs in the region of $n \approx 2 - 3$ for $P=12$ and $n \approx 10-20$ for $P=100$. On the other hand, the classical motion (T_1) and revival (T_2) dynamics are only marginally separated in this region, compared to what is possible at higher quantum numbers, and one could argue that well-resolved classical motion is at the heart of the physics of revival phenomena.

D. Example of wave-packet dynamics

We consider a Gaussian-shaped wave packet,

$$\psi(x,t=0) \propto \exp\left[-\frac{(x-x_0)^2}{2\sigma^2} + i\frac{p_x(x-x_0)}{\hbar} \right], \quad (19)$$

excited in a well of strength $P=100$ with $n_{max}=64$ bound levels. Initially, the packet is in the center of the well ($x_0=0$), with width $\sigma=0.07L$ and momentum $p_x=40\pi\hbar/L$. This wave packet is a superposition of approximately 20 energy levels centered around $\bar{n}=40$ [15]. This corresponds to a mean scaled action $\alpha_{\bar{n}}^- \approx 62.161$ and wave packet time scales $T_1 \approx 0.016\,293$, $T_2/2 \approx 40.4T_1$, $T_3/3 \approx 854T_2$, and $T_4/4 \approx 10.3T_3$. Note that the inequalities $T_1 \ll T_2/2! \ll T_3/3!$ are well satisfied by this wave packet; the inequality $T_3/3! \ll T_4/4!$ is satisfied but not strongly. We study the dynamics of this wave packet via the autocorrelation function

$$|C(t)|^2 = |\langle\psi(t)|\psi(0)\rangle|^2 = \left| \sum_{n=1}^{n_{max}} |c_n|^2 e^{-iE_n t/\hbar} \right|^2, \quad (20)$$
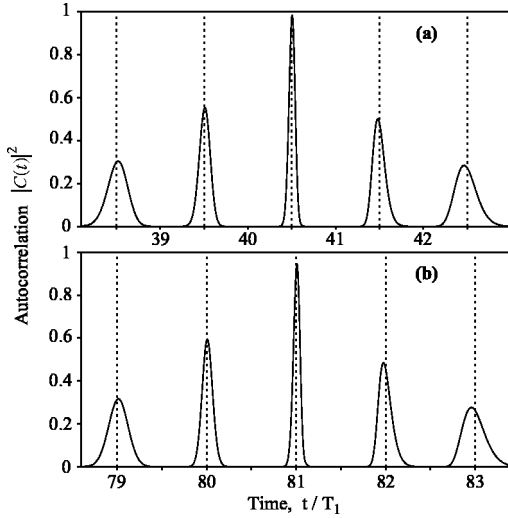
as is common in the literature [16].

FIG. 6. Revival dynamics: autocorrelation function $|C(t)|^2$ of the Gaussian wave packet described in Sec. III D, during (a) the first revival ($r=1$) and (b) the second revival ($r=2$). The dashed vertical lines are drawn at times given by Eq. (21), when revivals are predicted to occur.

1. Classical motion

At times $t \ll T_2$, the wave-packet evolution (9) is described approximately with a first-order truncation of the energy spectrum (1). This predicts periodic motion with classical period T_1. The autocorrelation function, plotted in Fig. 5, shows strong peaks at multiples of T_1. Although the wave packet spreads as it moves back and forth in the well due to the nonlinearities in the energy spectrum, its underlying periodic motion is still readily apparent.

2. Revivals

At times $t \ll T_3$, the wave-packet evolution (9) is described approximately with a quadratic truncation of the energy spectrum (1). Broadly speaking, there are wave-packet revivals at multiples of time $T_2/2$. Specifically, it has been shown [17] that when the semiclassical time-scale hierarchy is satisfied, wave-packet reformations are predicted at times

$$t_{\mathrm{rev}}(c,r) = \left(\left[\mathrm{rnd}\!\left(\frac{rT_2}{2T_1} \right) + c \right] + \left[\frac{r\,(\mathrm{mod}\,2)}{2} \right] \right) T_1 \quad (21)$$

[with rnd(x) equal to the integer closest to x, and $r\,(\mathrm{mod}\,m)$ equal to the integer between 0 and $m-1$ that is congruent to r modulo m], for small integers c and r serving as indices for the classical periods and revivals, respectively. The autocorrelation function (Fig. 6) shows that the wave packet correlates strongly with its original shape at the first two revivals. There is excellent agreement between the peaks in the autocorrelation function and the reformation times predicted by Eq. (21).

3. Super-revivals

At times $t \ll T_4$, the wave-packet evolution (9) is described approximately with a cubic truncation of the energy spectrum (1). Broadly speaking, there are wave-packet
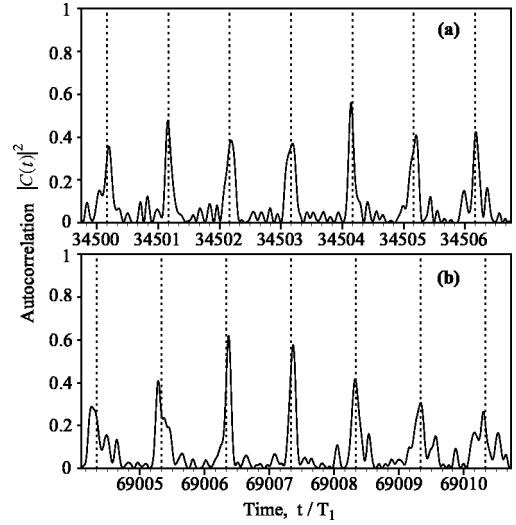

FIG. 7. Super-revival dynamics: autocorrelation function $|C(t)|^2$ of the Gaussian wave packet described in Sec. III D, during (a) the first revival near the first super-revival ($r=1, s=1$), and (b) the first revival near the second super-revival ($r=1, s=2$). The dashed vertical lines are drawn at times given by Eq. (22), when super-revivals are predicted to occur.

super-revivals at multiples of time $T_3/6$. Specifically, it has been shown [17] that when the semiclassical time-scale hierarchy is satisfied, wave-packet reformations are predicted at times

$$t_{\mathrm{sr}}(c,r,s) = \left(\left[\mathrm{rnd}\!\left(\left[\mathrm{rnd}\!\left(\frac{sT_3}{3T_2} \right) + r \right] \frac{T_2}{2T_1} \right) + c \right] \right.$$
$$\left. + \left[\frac{\mathrm{rnd}\!\left(\dfrac{sT_3}{3T_2} \right) + r\,(\mathrm{mod}\,2)}{2} \right] + \left[\frac{s\,(\mathrm{mod}\,6)}{6} \right] \right) T_1,$$
$$(22)$$

for small integers c, r, and s serving as indices for the classical periods, revivals, and super-revivals, respectively. The autocorrelation function (Fig. 7) shows that the wave packet reaches only 40–60% correlation with its initial shape during the first two super-revivals, although we note that these peaks are comparable to those seen at times T_1 and $2T_1$ in Fig. 5. Again there is excellent agreement between the peaks in the autocorrelation function and the reformation times predicted by Eq. (22).

IV. ''UNIVERSAL'' REVIVALS AND THE BOTTOM OF THE WELL

The universality of revivals in the *infinite* square well arises mathematically from the exact quadratic dependence of the energy, $E_n = E_1 n^2$. Physically, this originates from the complete confinement of the energy eigenstates inside the well. Just as the standing waves of a stretched string (with perfectly secured ends) oscillate with frequencies at exact harmonics of the fundamental mode and allow for disper-

sionless wave-packet propagation, the energy eigenmodes of the infinite square well (with perfectly confining boundaries) have phase oscillations with frequencies at harmonics of the ground state and allow for universal revival phenomena. In the *finite* square well, low-energy eigenstates are largely confined inside the square well, whereas high-energy eigenstates penetrate appreciably outside. Heuristically, then, we expect the closest analogy to infinite square-well wave-packet dynamics to occur at the bottom of the finite well.

In Sec. IV A we explore the bottom-of-the-well limit of the mean-quantum-number energy expansion (11) and show its connection with the infinite square well. For modest values of well strength (e.g., $P \leq 100$), there are noticeable inaccuracies in the predictions of this universal limit. In Sec. IV B we compare this limit more carefully with the mean-quantum-number expansion and address the difficulty (raised in Sec. III C) of separating the classical (T_1) and revival (T_2) dynamics near the well bottom.

A. "Universal" revival limit

At the very bottom of the finite square well (for $\alpha_n^- = 0$ and $\bar{n} = 0$), the energy expansion (11) reduces to

$$E_n = 2\pi\hbar\left[\frac{n^2}{\tau_2} - \frac{n^4}{\tau_4} - \frac{n^6}{\tau_6} - \cdots\right], \qquad (23)$$

with times

$$\tau_2 = \frac{4}{\pi}\frac{(P+1)^2}{P^2}, \qquad (24)$$

$$\tau_4 = \frac{48}{\pi^3}\frac{(P+1)^5}{P^2}, \qquad (25)$$

and so forth. Note that the time scales in Eq. (23) are related to those in Eq. (11) with

$$\tau_j = T_j(\alpha_n^- = 0), \qquad (26)$$

and that the odd-index times (τ_1, τ_3, etc.) diverge at the bottom of the well and are removed from the energy expansion. In practice, Eq. (23) is most useful for small scaled actions ($\alpha_n^- \ll P$) or alternately, small quantum numbers ($\bar{n} \ll n_{\max}$) [18].

Equation (23) generalizes the form of Eq. (2) and describes universal revival phenomena in the finite well, since the time scales τ_j depend only on the well-strength parameter P. In the infinite square-well limit ($P \to \infty$), the revival time is $\tau_2 = 4/\pi$ and the higher-order times (τ_4, τ_6, etc.) diverge, in agreement with previous results [7,8,19].

1. Short-time universal revival model: Connections with the infinite square well

At times $t \ll \tau_4$, the wave-packet evolution (9) at the bottom of the well is described approximately with a quadratic truncation of the energy spectrum (23) as
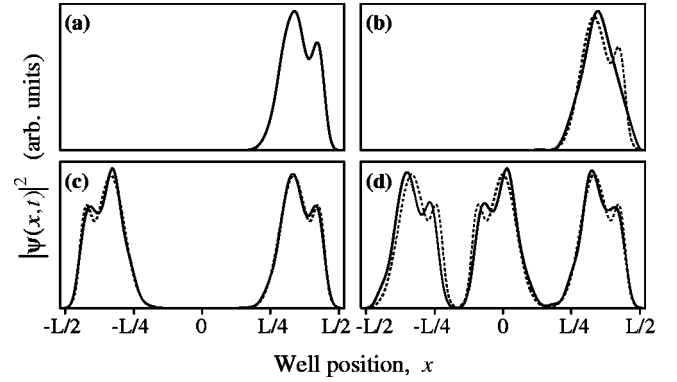

FIG. 8. Fractional and full revivals: probability densities $|\psi(x,t)|^2$ of (a) an initial wave packet (mean quantum number $\bar{n} = 3$), centered at $x_0 = L/3$ and excited in a well of depth $P = 50$; (b) the first revival of this wave packet at time T_2; (c) the 1/2 fractional revival at time $T_2/4$; and (d) the 1/3 fractional revival at time $T_2/3$. The light dashed lines correspond to the wave-packet shapes expected in the infinite square-well ($P \to \infty$) limit. Note that the finite-well fractional and full revivals do not reproduce the original wave-packet shape with the same fidelity seen in the infinite-well limit because of the higher-order terms in the energy spectrum (23), or alternately, because of the penetration of the finite-well eigenstates $\phi_n(x)$ beyond the well boundaries.

$$\psi(x,t) \approx \sum_{n=1}^{n_{\max}} \exp[-i2\pi(t/\tau_2)n^2]c_n\phi_n(x). \qquad (27)$$

As was first noted by Venugopalan and Agarwal [8], this has the same form as the equation describing dynamics in the infinite square well [c.f. Ref. [7], Eq. (9)], with the finite-well revival time differing from the infinite-well revival time by the scaling factor $(P+1)^2/P^2$. The cycle of fractional and full revivals we found for the infinite square well [7] carry over directly to finite wells (for example, see Fig. 8) within the time-limit restriction.

2. Accuracy and limitations of universal predictions

We revisit an example considered by Venugopalan and Agarwal [8] of an initial Gaussian wave packet in the form of Eq. (19), with mean position $x_0 = L/5$, width $\sigma = L/10$, and momentum $p_x = 0$, excited in a well of depth $P = 12$. This wave packet is centered around energy level $\bar{n} = 2$ in a well with $n_{\max} = 8$ levels. Note that the universal revival limit condition of validity $\bar{n} \ll n_{\max}$ is not well satisfied here; in fact, *no* wave packet can rigorously satisfy this condition in such a shallow well. Thus this example offers insights into both the accuracy and the limitations of the universal revival limit.

At times $t \ll \tau_4$, Eq. (27) predicts wave-packet revivals at multiples of time τ_2. Broadly speaking, the autocorrelation function (Fig. 9) shows the expected peaks at these times. Note that the peaks at $\tau_2/3$ and $2\tau_2/3$ in Fig. 9 are caused by an interesting effect in the wave packet's *fractional* revivals: two of the three subpackets in the spatial wave function during the $\frac{1}{3}$ and $\frac{2}{3}$ fractional revivals overlap, interfere constructively, and correlate strongly with the initial packet.
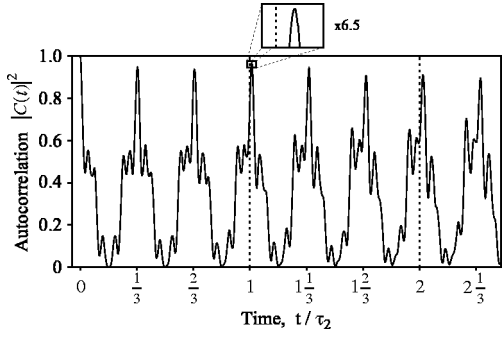
FIG. 9. Test of universal revival limit: autocorrelation function $|C(t)|^2$ of the Gaussian wave packet described in Sec. IV A 2, during the first two revival periods. The dashed vertical lines are drawn at multiples of τ_2, the predicted revival time in the universal limit.

There are, however, noticeable differences between predicted and exact revival peaks (Fig. 9, magnified inset). Venugopalan and Agarwal studied these time differences in detail (Ref. [8], Table I) and showed that they diminish rapidly with increasing well-strength parameter. Although the error is only 0.9% in Fig. 9, we have still lost the high degree of accuracy enjoyed in Sec. III D.

B. Comparison with mean-quantum-number predictions

The mean-quantum-number revival formalism is mathematically valid at the bottom of the well, but the difficulty in separating the classical motion and revival dynamics prevents a simple physical interpretation of its predictions. The universal revival limit offers a greatly simplified picture of the dynamics at the well bottom, but there are small time differences between the peaks in the autocorrelation function and the predicted revival times at multiples of time τ_2. In this section, we show that these revival-time differences can be understood with a careful analysis of the mean-quantum-number expansion (1).

The time scales T_j [Eqs. (12)–(14)] are analytic functions of the mean scaled action $\alpha_{\bar{n}}$, and can be described at the bottom of the well as a power series in the mean quantum number $\bar{n}$ with the help of Eq. (23). We find that the classical motion time is

$$T_1 = \frac{(P+1)^2}{P^2}\left[\frac{1}{(\bar{n}\pi/2)} + \frac{2}{3(P+1)^3}\left(\frac{\bar{n}\pi}{2}\right) + \cdots\right], \quad (28)$$

and the revival time is

$$T_2 = \frac{4}{\pi}\frac{(P+1)^2}{P^2}\left[1 + \frac{2}{(P+1)^3}\left(\frac{\bar{n}\pi}{2}\right)^2 + \cdots\right]. \quad (29)$$

The mean-quantum-number description and its universal limit agree (for times $t \ll T_3$ or $t \ll \tau_4$) when we use only the leading terms in T_1 and T_2; the higher-order terms are the corrections from universality.

In Sec. III C, we noted that the inequality $T_1 \ll T_2/2!$ does not hold at the bottom of the well, so the revival-time predictions of Eq. (21) are not valid. The time scales T_1 and T_2,
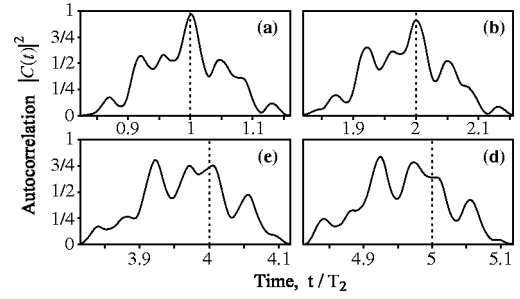

FIG. 10. Test of mean-quantum-number revival predictions: autocorrelation function $|C(t)|^2$ of the Gaussian wave packet described in Sec. III D. Near times (a) T_2 and (b) $2T_2$ there are revivals at the predicted times. Near times (c) $4T_2$ and (d) $5T_2$ we confirm the estimate of Eq. (31), that the revival times are not simple multiples of time T_2 once the noninteger nature of the ratio T_2/T_1 becomes significant.

however, are both much smaller than T_3, so for times $t \ll T_3$ the wave-packet dynamics is still governed by a quadratic truncation of the energy spectrum (1). Recall that in the infinite well, these times satisfy $T_2/T_1 = 2\bar{n}$. This generalizes at the bottom of the finite well [using Eqs. (28) and (29)] to

$$\frac{T_2}{T_1} = 2\bar{n} + \frac{2\pi^2}{3(P+1)^3}\bar{n}^3 + \cdots. \quad (30)$$

Thus the time scale T_2 is nearly an integer multiple of T_1, and we expect quasiperiodic dynamics, with period T_2, until the higher-order terms in Eq. (30) become significant. Figures 10(a) and 10(b) show that the first few revivals do coincide with multiples of T_2. Thus the revival-time differences noted above are precisely the differences $T_2 - \tau_2$ between the mean-quantum-number and universal descriptions of revivals.

This simple picture, of approximately synchronized classical motion and revival-time scales, breaks down at the jth revival when the ratio jT_2/T_1 has drifted by a small fraction of an integer. A good "rule of thumb" is that this breakdown occurs when

$$\frac{2\pi^2 j}{3(P+1)^3}\bar{n}^3 \approx \frac{1}{10}. \quad (31)$$

For the wave packet considered in Sec. IV A 2, this estimates a breakdown at $\approx 4.2T_2$. In Figs. 10(c) and 10(d), we confirm that the autocorrelation peaks no longer coincide with multiples of T_2 at the fourth and fifth revival.

Beyond the breakdown of the T_2-periodic dynamics described by Eq. (31), the failure of the time-scale hierarchy at the bottom of the well impedes predictions of subsequent wave-packet reformations as functions of T_1 and T_2, which were possible in Sec. III D 3. The dynamics of a specific wave packet can be studied numerically in terms of amplitudes c_n and square-well energies E_n, but we do not know if a more robust analytic description is possible at the bottom of the well for these longer times.

We note that for the wave packet analyzed in Sec. IV A 2, we predict poorly resolved super-revivals in the vicinity of time $T_3/6 \approx 73.6$. Venugopalan and Agarwal [8] searched for

the first super-revival of this wave packet by looking for local maxima in the autocorrelation function and estimated that this occurs much sooner, at time $15 \times (4/\pi) \approx 19.1$. With the mean-quantum-number revival interpretation, we believe that they found maxima in the beating between the T_1 and T_2 dynamics, in a regime before the effects of T_3 were significant.

[1] Such ''classical limit'' states of hydrogen were first examined by L.S. Brown, Am. J. Phys. **41**, 525 (1973); Analysis of the classical dynamics of electron wave packets formed by picosecond laser pulses in Rydberg atoms was presented by J. Parker and C.R. Stroud, Jr., Phys. Scr. **T12**, 70 (1986).

[2] Revivals of Rydberg atomic-electron wave packets were discovered by J. Parker and C.R. Stroud, Jr., Phys. Rev. Lett. **56**, 716 (1986); The general theory of fractional revivals was developed by I.Sh. Averbukh and N.F. Perelman, Phys. Lett. A **139**, 449 (1989).

[3] Super-revivals of Rydberg wave packets have been examined, for example, by R. Bluhm and V.A. Kostelecký, Phys. Lett. A **200**, 308 (1995); and R. Bluhm and V.A. Kostelecký, Phys. Rev. A **51**, 4767 (1995).

[4] Revival phenomena in systems with two quantum numbers have been considered, for example, by R. Bluhm, V.A. Kostelecký, and B. Tudose, Phys. Lett. A **222**, 220 (1996); G.S. Agarwal and J. Banerji, Phys. Rev. A **57**, 3880 (1998); and J. Banerji and G.S. Agarwal, Opt. Express **5**, 220 (1999).

[5] C. Leichtle, I.Sh. Averbukh, and W.P. Schleich, Phys. Rev. Lett. **77**, 3999 (1996); C. Leichtle, I.Sh. Averbukh, and W.P. Schleich, Phys. Rev. A **54**, 5299 (1996).

[6] D.J. Griffiths, *Introduction to Quantum Mechanics* (Prentice-Hall, Englewood Cliffs, NJ, 1995), pp. 24–29.

[7] D.L. Aronstein and C.R. Stroud, Jr., Phys. Rev. A **55**, 4526 (1997).

[8] A. Venugopalan and G.S. Agarwal, Phys. Rev. A **59**, 1413 (1999).

[9] For example, see H.C. Ohanian, *Principles of Quantum Mechanics* (Prentice-Hall, Englewood Cliffs, NJ, 1990), pp. 78–84; R.L. Liboff, *Introductory Quantum Mechanics*, 2nd ed. (Addison-Wesley, Reading, MA, 1992), pp. 275–284; and S. Gasiorowicz, *Quantum Physics*, 2nd ed. (Wiley, New York, 1996), pp. 78–83.

[10] B.I. Barker, G.H. Rayborn, J.W. Ioup, and G.E. Ioup, Am. J. Phys. **59**, 1038 (1991).

[11] D.W.L. Sprung, H. Wu, and J. Martorell, Eur. J. Phys. **13**, 21 (1992).

[12] P.M. Morse and H. Feshbach, *Methods of Theoretical Physics* (McGraw-Hill, New York, 1953), Vol. 1, pp. 411–413; *Handbook of Mathematical Functions* edited by M. Abramowitz and I.A. Stegun (Dover, New York, 1972), p. 16.

[13] Z.D. Gaeta and C.R. Stroud, Jr., Phys. Rev. A **42**, 6308 (1990).

[14] D.W.L. Sprung, H. Wu, and J. Martorell, Am. J. Phys. **64**, 136 (1996).

[15] The mean quantum number was computed with the formula $\bar{n} = \mathrm{int}(\Sigma_n |c_n|^2 n)$. The results of Knospe and Schmidt [17], used in Secs. III D 1–III D 3, require that the value of $\bar{n}$ be restricted to integer values.

[16] Visualizing quantum dynamics via the autocorrelation function has been emphasized in research into semiclassical (Van Vleck-Gutzwiller) methods; for example, see S. Tomsovic and E.J. Heller, Phys. Rev. Lett. **67**, 664 (1991). Physically, the autocorrelation function is important because it is directly related to the ionization signal in pump-probe experiments.

[17] O. Knospe and R. Schmidt, Phys. Rev. A **54**, 1154 (1996).

[18] The energy spectrum at the well bottom was computed by Barker *et al.* [10] and by Sprung, Wu, and Martorell [11]. These authors give numerical examples comparing the predictions of Eq. (23) with the exact values of energy, and the series solution is found to converge very rapidly at the bottom of the well. Here we are concerned with the related issue of how truncating Eq. (23) affects predictions of the *dynamics* in the square well.

[19] R. Bluhm, V.A. Kostelecký, and J.A. Porter, Am. J. Phys. **64**, 944 (1996).